GEOPHYSICS. VOL. 77, NO. 1 (JANUARY-FEBRUARY 2012); P. H1–H7, 6 FIGS.
10.1190/GEO2011-0054.1

Accounting for soil surface roughness in the inversion of ultrawideband off-ground GPR signal for soil moisture retrieval

François Jonard[1], Lutz Weihermüller[1], Harry Vereecken[1], and Sébastien Lambot[2]

ABSTRACT

We combined a full-waveform ground-penetrating radar (GPR) model with a roughness model to retrieve surface soil moisture through signal inversion. The proposed approach was validated under laboratory conditions with measurements performed above a sand layer subjected to seven different water contents and four different surface roughness conditions. The radar measurements were performed in the frequency domain in the range of 1–3 GHz and the roughness amplitude standard deviation was varied from 0 to 1 cm. Two inversion strategies were investigated: (1) Full-waveform inversion using the correct model configuration, and (2) inversion focused on the surface reflection only. The roughness model provided a good description of the frequency-dependent roughness effect. For the full-waveform analysis, accounting for roughness permitted us to simultaneously retrieve water content and roughness amplitude. However, in this approach, information on soil layering was assumed to be known. For the surface reflection analysis, which is applicable under field conditions, accounting for roughness only enabled water content to be reconstructed, but with a root mean square error (RMS) in terms of water content of 0.034 $\mathrm{m^3\,m^{-3}}$ compared to an RMS of 0.068 $\mathrm{m^3\,m^{-3}}$ for an analysis where roughness is neglected. However, this inversion strategy required a priori information on soil surface roughness, estimated, e.g., from laser profiler measurements.

INTRODUCTION

Knowledge of surface water content is essential in the fields of agricultural and environmental engineering, hydrology, meteorology, and climatology (Vereecken et al., 2008; Seneviratne et al., 2010). As the dielectric permittivity of liquid water dominates the dielectric permittivity of other soil components, water is the principal factor governing electromagnetic wave propagation in the soil. This allows us to use geophysical techniques to indirectly measure the surface water content of the soil (Ulaby et al., 1982). Many studies have investigated the potential of microwave radar systems to monitor the spatio-temporal variation of the surface and subsurface soil water content. Spaceborne and airborne synthetic aperture radars (SAR) yield soil moisture estimates on a large spatial scale (1–100 km), which are particularly relevant for catchment-scale studies (Moran et al., 2004). At the field scale, ground-penetrating radar (GPR) has proven to be successful in many hydrological applications. Reviews on the uses and recent developments of GPR are given by Huisman et al. (2003) and Slob et al. (2010). Compared to local measurements such as soil sampling and time-domain reflectometry (TDR), GPR has the advantage of allowing noninvasive quantification of soil properties with a high spatial resolution at the field scale. Lambot et al. (2004b) proposed a full-waveform forward and inverse modeling approach which applies to off-ground GPR. The electromagnetic model is based on a solution of the 3D Maxwell equations for waves propagating in multilayered media and correctly accounts for antenna effects and antenna-soil interactions. The model was shown to be applicable for reproducing the radar measurements, and model inversion was successfully applied to identify and map surface soil moisture in the field (Jonard et al., 2011). Electromagnetic wave reflection on a bare soil is highly dependent on the surface roughness. A distinction can be made between smooth and rough surfaces with respect to the wavelength of the signal based on the Rayleigh criterion ($h_c = \lambda/8\,\cos(\gamma)$, where h_c is the critical height of the

Manuscript received by the Editor 15 February 2011; revised manuscript received 22 June 2011; published online 3 February 2012.

[1]Institute of Bio- and Geosciences, Research Centre Jülich, Jülich, Germany. E-mail: f.jonard@fz-juelich.de; l.weihermueller@fz-juelich.de; h.vereecken@fz-juelich.de.

[2]Institute of Bio- and Geosciences, Research Centre Jülich, Jülich, Germany; Université catholique de Louvain, Earth and Life Institute, Louvain-la-Neuve, Belgium. E-mail: sebastien.lambot@uclouvain.be.

surface protuberances, γ is the incidence angle, and λ is the wavelength) (Ulaby et al., 1982). If the surface is smooth and homogeneous (in terms of electrical properties), most of the energy reflected will be in the specular direction (coherent component), while if the surface is rough, diffuse reflections or scattering (incoherent component) can occur leading to less energy being recorded in the specular direction. These diffuse reflections and the reduction of energy in the specular direction should be accounted for to accurately retrieve the surface soil moisture. Previous studies carried out with airborne and spaceborne remote sensing radars also demonstrated the need to take surface roughness into account in signal processing for soil moisture retrieval (Quesney et al., 2000; Baghdadi et al., 2008; Verhoest et al., 2008). The roughness effect has also been shown for GPR (Sai and Ligthart, 2004; Yarovoy et al., 2004; Lambot et al., 2006a; Giannopoulos and Diamanti, 2008; van der Kruk et al., 2010). Nevertheless, the issue remains poorly investigated for the retrieval of the soil electromagnetic properties by off-ground GPR, and no GPR model accounting for roughness is currently available in the literature. In this paper, we combine the full-waveform GPR model of Lambot et al. (2004b) with the Ament roughness model derived from the Kirchhoff scattering theory (Ament, 1953; Beckmann and Spizzichino, 1987) to retrieve surface soil moisture through signal inversion. To account for surface roughness, the global surface reflection coefficient is multiplied by a scattering loss factor. The proposed approach was validated under laboratory conditions with measurements performed above a sand layer subjected to seven different water contents and four different surface roughness conditions. Numerical experiments were also performed to analyze the well-posedness of the inverse problem.

EXPERIMENT

Experimental setup

Radar measurements were performed under laboratory conditions above a rectangular wooden container (1.45×1.30 m^2 area) homogeneously filled with a sand layer 0.09 m in thickness (Figure 1) (Lambot et al., 2006a). Below the sand layer, a horizontal metal sheet was installed to control the bottom boundary condition in the electromagnetic model. Indeed, materials underneath this metal sheet have no influence on the measured backscattered signal. The sand was subjected to seven different water contents ranging from dry to wet conditions (θ_i with $i = 1$ to 7) and four different surface roughness heights (R_j with $j = 1$ to 4), including a smooth surface (R_1), resulting in 28 independent configurations ($\theta_i R_j$). For each water content level, the sand was mixed manually to obtain a homogeneous distribution of the water within the whole sand layer and the desired roughness topographies were produced by pressing a cylinder with stones randomly glued onto the surface over the smooth sand surface. Independent surface roughness characterization was performed using a 1 m long mechanical needle-like profiler.

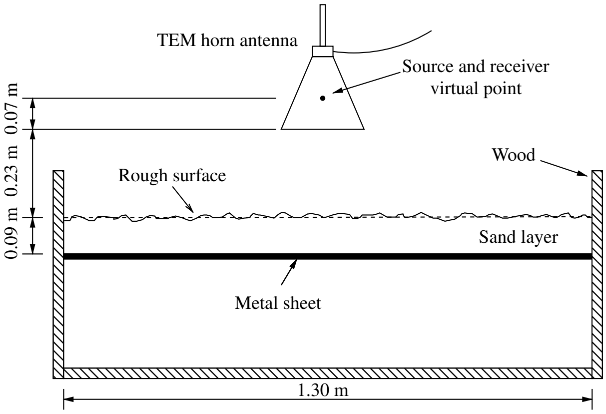

Figure 1. Laboratory experimental setup including the sand box made of wood, the off-ground horn antenna, the sand layer subject to different water content and roughness conditions, and a metal sheet at the bottom to control the boundary condition in the electromagnetic model (Lambot et al., 2006a).

Radar system

The radar system was set up using a vector network analyzer (VNA, ZVRE, Rohde and Schwarz, Munich, Germany) as transmitter and receiver, thereby providing an ultrawideband stepped-frequency continuous-wave system. The antenna system consisted of a linear polarized double-ridged broadband horn antenna (BBHA 9120 D, Schwarzbeck Mess-Elektronik, Schönau, Germany). Antenna dimensions were 22 cm length and 14×24 cm^2 aperture area, and the -3 dB full beamwidth of the antenna was 27° in the E-plane and 22° in the H-plane (at 2 GHz). The antenna nominal frequency range is 1–18 GHz and its isotropic gain ranged from 6 to 18 dBi. Measurements were performed with the antenna aperture situated at an average height of 23 cm above the soil surface with a normal incidence (Figure 1) and by operating frequencies over the range 1–3 GHz (4 MHz step).

MODELS

Radar model

The raw GPR data consist of the frequency-dependent complex ratio $S_{11}(\omega)$ between the backscattered electromagnetic field ($b(\omega)$) and the incident electromagnetic field ($a(\omega)$), with ω being the angular frequency. Assuming the distribution of the electromagnetic field measured by the antenna to be independent of the scatterer, i.e., only the phase and amplitude of the field change (plane wave approximation over the antenna aperture), the following equation is applied to filter out the antenna effects (Lambot et al., 2004b):

$$S_{11}(\omega) = \frac{b(\omega)}{a(\omega)} = H_{\mathrm{i}}(\omega) + \frac{H(\omega) G^{\uparrow}_{\mathrm{xx}}(\omega)}{1 - H_{\mathrm{f}}(\omega) G^{\uparrow}_{\mathrm{xx}}(\omega)} \qquad (1)$$

where $H_{\mathrm{i}}(\omega)$ is the antenna return loss, $H(\omega)$ is the antenna transmitting-receiving transfer function, $H_{\mathrm{f}}(\omega)$ is the antenna feedback loss, and $G^{\uparrow}_{\mathrm{xx}}(\omega)$ is the transfer Green's function of the air-soil system. The Green's function represents a solution of the 3D Maxwell equations for electromagnetic waves propagating in multilayered media (Michalski and Mosig, 1997). We derived this specific Green's function using a recursive scheme to compute the transverse electric (TE) and magnetic (TM) global reflection coefficients of the multilayered medium in the spectral domain (Slob and Fokkema, 2002). The transformation back to the spatial domain is performed by numerically evaluating a semi-infinite, complex integral (Lambot et al., 2007). The characteristic antenna transfer functions can be determined by solving a system of equations such as (1) to the unknowns $H_{\mathrm{i}}(\omega)$, $H(\omega)$, and $H_{\mathrm{f}}(\omega)$ for different well-defined model configurations, i.e., with the antenna at different heights above a perfect electrical conductor (PEC). The Green's functions can therefore be computed and $S_{11}(\omega)$ can be measured readily.

Full-waveform inverse modeling of the GPR data was performed in the frequency domain to identify the electromagnetic properties (i.e., the relative permittivity ε_{r} (dimensionless) and the electrical conductivity σ ($\mathrm{S\,m^{-1}}$)) of the soil (Lambot et al., 2004b). The inverse problem was formulated in the least-squares sense and the objective function to be minimized was accordingly defined as follows

$$\phi_1(\mathbf{b}) = |\mathbf{G}^{\uparrow *}_{\mathrm{xx}} - \mathbf{G}^{\uparrow}_{\mathrm{xx}}|^T\,|\mathbf{G}^{\uparrow *}_{\mathrm{xx}} - \mathbf{G}^{\uparrow}_{\mathrm{xx}}| \quad (2)$$

where $\mathbf{G}^{\uparrow *}_{\mathrm{xx}}(\omega)$ and $\mathbf{G}^{\uparrow}_{\mathrm{xx}}(\mathbf{b},\omega)$ are, respectively, the measured and modeled Green's functions in the frequency domain, and $\mathbf{b}$ is the parameter vector to be estimated (e.g., $\mathbf{b} = [\varepsilon_{\mathrm{r}}, \sigma]$, depending on the unknowns). Because the Green's functions are complex vectors, the difference between observed and modeled data is expressed by the magnitude of the errors in the complex plane, thereby inherently accounting for amplitude and phase information. Optimization was performed using the global multilevel coordinate search (GMCS) algorithm (Huyer and Neumaier, 1999) combined sequentially with the local Nelder-Mead simplex algorithm (NMS) (Lagarias et al., 1998) as proposed by Lambot et al. (2004a). For this inversion, the distance between the soil surface and the metal sheet h (m) was assumed to be known (Figure 1).

Inversion in the time domain also was performed by focusing on a time window containing the surface reflection only (Lambot et al., 2006b; Jonard et al., 2011). The measured and modeled frequency domain Green's functions were first transformed in the time domain using the inverse Fourier transform. The inverse problem consisted of finding the minimum of the following objective function

$$\phi_2(\mathbf{b}) = (\mathbf{g}^{\uparrow *}_{\mathrm{xx}} - \mathbf{g}^{\uparrow}_{\mathrm{xx}})^T\,(\mathbf{g}^{\uparrow *}_{\mathrm{xx}} - \mathbf{g}^{\uparrow}_{\mathrm{xx}}) \quad (3)$$

where $\mathbf{g}^{\uparrow *}_{\mathrm{xx}}(\mathbf{t})$ and $\mathbf{g}^{\uparrow}_{\mathrm{xx}}(\mathbf{b},\mathbf{t})$ are, respectively, the measured and modeled Green's functions in the time domain. Optimization was performed using the local Levenberg-Marquardt algorithm (Marquardt, 1963).

A sand-specific empirical model (third-order polynomial) derived in Lambot et al. (2006a) was used to relate GPR-derived relative dielectric permittivity to the volumetric water content θ

$$\begin{aligned}\theta = {} & 2.30\times10^{-4}\varepsilon_{\mathrm{r}}^3 - 6.28\times10^{-3}\varepsilon_{\mathrm{r}}^2 \\ & + 7.50\times10^{-2}\varepsilon_{\mathrm{r}} - 1.51\times10^{-1}\end{aligned} \quad (4)$$

Surface roughness model

In general, the surface is assumed to be stationary with a random Gaussian height distribution. The soil surface can therefore be described by the following statistical quantities: the standard deviation of the surface height s_r (m), the spatial autocorrelation function, and the spatial correlation length (Fung et al., 1992).

To account for roughness effects on radar electromagnetic wave propagation, the Ament model (Ament, 1953; Beckmann and Spizzichino, 1987) was used. This model, which is derived from the Kirchhoff scattering theory, describes the scattering losses in the specular direction due to the reflection on a rough interface. This model has been applied in several studies investigating the roughness effect on electromagnetic wave scattering, e.g., by Pinel et al. (2007) for radar reflection over sea surfaces and Landron et al. (1996) for radar reflection on rough building materials. In this model, the global surface reflection coefficient is multiplied by a scattering loss factor (ρ), which is based on the Rayleigh parameter as a function of frequency, namely,

$$\rho = e^{-\frac{g}{2}} \quad (5)$$

with

$$g = \left(\frac{4\pi s_r \cos\gamma_i}{\lambda}\right)^2 \quad (6)$$

where s_r is the standard deviation of the surface height, γ_i is the angle of incidence, and λ is the free space wavelength of the incident wave. The modified reflection coefficient R^{R} that models the reduction of the signal power in the specular direction is then defined as

$$R^{\mathrm{R}}_{\mathrm{TE}} = \rho R^{\mathrm{F}}_{\mathrm{TE}} \quad (7)$$

$$R^{\mathrm{R}}_{\mathrm{TM}} = \rho R^{\mathrm{F}}_{\mathrm{TM}} \quad (8)$$

where $R^{\mathrm{F}}_{\mathrm{TE}}$ and $R^{\mathrm{F}}_{\mathrm{TM}}$ are, respectively, the global TE- and TM-mode surface reflection coefficients for a smooth surface. Equations 7 and 8 assume that the surface heights have a Gaussian distribution with negligible sharp edge and shadowing effects. The model also assumes that there is no multiple scattering (Beckmann and Spizzichino, 1987). In our case, the incidence is normal ($\gamma_i = 0$) and the model is applied to the spectral-domain global reflection coefficients of the first interface (sand surface) of the 3D layered medium.

RESULTS AND DISCUSSION

Response surface analysis

To analyze the well-posedness of the inverse problem, we calculated response surfaces of the objective function using synthetic error-free data and real data. Real data correspond to intermediate water content and roughness conditions ($\theta = 0.14\ \mathrm{m^3\,m^{-3}}$; $s_r =$ 0.49 cm), but similar results were obtained for the other conditions. Inversions were performed in a relatively large parameter space ($2 < \varepsilon_{\mathrm{r}} < 12$; $0 < h < 0.25$ m; $1\times10^{-5} < \sigma < 1\times10^{-1}\ \mathrm{S\,m^{-1}}$; $0 < s_r < 0.025$ m), which contained the exact solutions. The range of each parameter was divided into 200 discrete values resulting in 40,000 objective function values for each contour plot.

Figure 2 shows the response surfaces of the logarithm of the objective function values in four parameter planes ε_{r}-h, h-s_r, σ-s_r, and ε_{r}-s_r and for the full-waveform inversion case (equation 2). For the synthetic data (left panel), each response surface shows a well-defined global minimum, which reveals that sufficient information is contained in the inverse problem to estimate the parameters of interest simultaneously. In the ε_{r}-h parameter plane, the global minimum region exhibits a banana shape, which suggests an important negative correlation between these parameters. A similar signal can indeed be obtained for either a low dielectric permittivity with a high-layer thickness, or a high dielectric permittivity with a

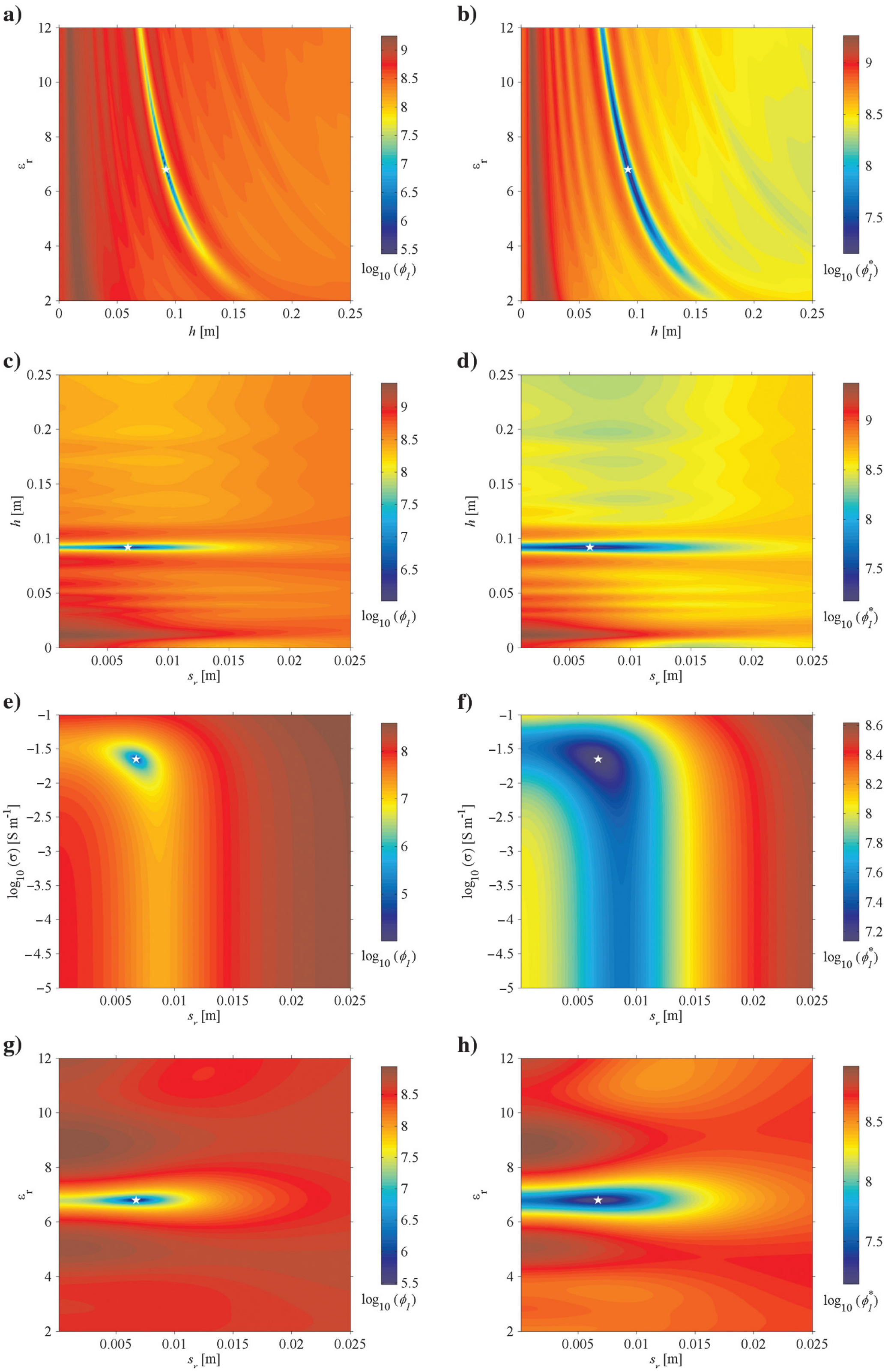

Figure 2. Response surfaces of the objective function logarithm $\log_{10}(\phi_1(\mathbf{b}))$ for the full-waveform inversion in the ε_r-h (a), h - s_r (b), ε_r-s_r (c), and σ-s_r (d) parameter planes. Left plots correspond to numerically generated error-free data ($\phi_1(\mathbf{b})$), and right plots correspond to real data ($\phi_1^*(\mathbf{b})$). The asterisk represents the global minimum of the objective function. Note that the color scale differs for the single response surfaces.

low-layer thickness. The h-s_r and ε_r-s_r response surfaces show an elliptical global minimum region parallel to the s_r axis. Additionally, local minimums can also be observed. In general, the response surfaces suggest that the two parameter pairs are uncorrelated. Indeed, s_r determines the attenuation of the wave while h and ε_r determine the propagation time of the wave throughout the layer. These parameters then independently determine the amplitude (s_r) and the phase (h or ε_r) of the radar electromagnetic waves propagating through the soil. In the σ-s_r parameter plane, no local minimums can be observed and the parameters are negatively correlated. In fact, a high σ will strongly attenuate the signal throughout the layer as well as a high s_r. Response surfaces pertaining to the real data (right panel) exhibit the same general shape as the synthetic response surfaces. For each parameter plane, the position of the global minimum is unchanged, which demonstrates the stability of the inverse problem with respect to measurement and modeling errors. As expected, the values of the objective function are systematically higher and the global minimum regions are flatter for the real data, resulting in an increase in parameter uncertainty (note that the color scale differs for the single response surfaces). In the ε_r-h parameter plane, given the negative correlation of the parameters and the larger global minimum region, compared to the synthetic case, an accurate estimation of ε_r will require a priori information about the layer thickness (h).

Figure 3 shows the response surfaces of the logarithm of the objective function (equation 3) in the ε_r-s_r parameter plane for the surface reflection inversion. Figures 3a and 3b show the response surface with synthetic data and real data, respectively. The synthetic response surface shows a well-defined minimum. However, for the real data, the values of the objective function are higher and the global minimum region is flatter, resulting in larger uncertainty in the estimation of the parameters. For both response surfaces, a significant positive correlation between s_r and ε_r can be observed. As a result, an increase in s_r has a similar effect on the objective function as a decrease in ε_r, which increases parameter estimation uncertainty. In fact, the reflection coefficient will decrease with an increase of the surface roughness or a decrease of the water content/dielectric permittivity. An accurate estimation of ε_r is therefore not possible without knowledge of any soil roughness parameters, especially for the real data case. Compared to the full-waveform inversion, this increase in uncertainty comes from the lower information content in the radar data when focusing on the surface reflection only. Indeed, for the surface reflection inversion, ε_r and s_r information is obtained from the surface reflection only. As a consequence, information about ε_r and s_r is correlated. For the full-waveform inversion, similar information is obtained from the surface reflection. However, information about ε_r is also obtained from the two-way travel time through the soil layer. This additional information allows us to estimate ε_r with higher accuracy and without a priori information about s_r. The surface reflection inversion strategy is particularly useful under field conditions for which layering is a priori unknown.

Green's functions

Figure 4 depicts the measured and modeled Green's function in the frequency domain for two different combinations of water content and roughness level (Figure 4a: $\theta = 0.15$ m^3 m^{-3}-$s_r = 0.33$ cm; Figure 4b: $\theta = 0.20$ m^3 m^{-3}-$s_r = 0.88$ cm). Other scenarios are similar and show intermediate results. Figure 4a and 4b show that the modeled amplitude of the Green's function does not fit measurements above 2 GHz if no roughness correction is applied for water content and roughness conditions. The modeled amplitude of the Green's function overestimates the measurements and this overestimation, as expected, increases with frequency. We observe that the roughness model describes this behavior relatively well, although some discrepancies remain due to oscillations in the Green's function amplitude that cannot be described by the scattering loss factor (exponential behavior only). Indeed, the scattering loss factor applied in this study accounts only for the reduction of energy in the specular direction. As a result, only the coherent component is assumed to contribute to the reflected signal. The remaining Green's functions oscillations could therefore be attributed to the contribution of the incoherent components. In both cases, the phase of the Green's function is properly reproduced and corresponds to the propagation times in air and sand layer.

Full-waveform inverse estimations

In Figure 5, the roughness standard deviation s_r measured by the needle-like profiler was compared to values inverted using the

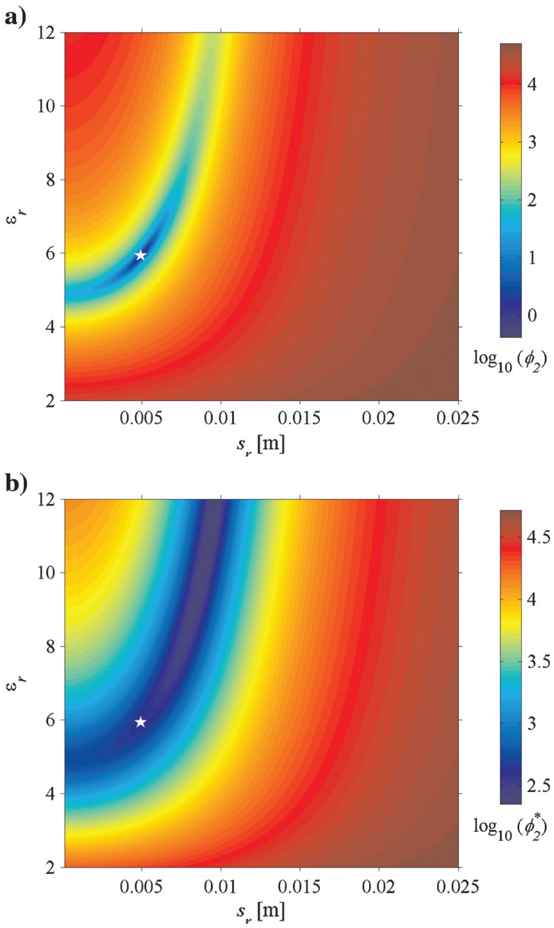

Figure 3. Response surfaces of the objective function logarithm $\log_{10}(\phi_2(\mathbf{b}))$ for the surface reflection inversion in the ε_r-s_r parameter plane using (a) numerically generated error-free data ($\phi_2(\mathbf{b})$), and (b) real data ($\phi_2^*(\mathbf{b})$). The asterisk represents the global minimum of the objective function. Note that the color scale differs for the two response surfaces.

full-waveform inversion (equation 2, $\mathbf{b} = [\varepsilon_r, \sigma, s_r]$). In total, twenty-one configurations (three roughness levels combined with seven water content levels) were analyzed. Although the inversion failed for one scenario ($\theta_2 R_2$), a relatively good agreement was obtained between the real and GPR-derived values (correlation coefficient $r^2 = 0.55$, root mean square error RMS $= 0.22$ cm). In general, inverted data slightly overestimated the measured s_r. To estimate the sand dielectric permittivity, the use of the roughness model did not improve the estimations compared to the smooth model. This is due to the fact that the permittivity information is not only contained in the surface reflection, but also in the two-way travel time between the sand surface and the underlying perfect electrical conductor. Only the estimation of the electrical conductivity was affected, which is due to energy loss by surface scattering.

Surface reflection inverse estimations

For this scenario, only the surface dielectric permittivity was inverted for (equation 3, $\mathbf{b} = [\varepsilon_r]$). The results for the largest roughness level (s_r between 0.6 and 1.0 cm) are presented in Figure 6 and are expressed in terms of water content using the sand-specific petrophysical relationship (equation 4). The errors in the estimation of water content are presented for both models. The errors are defined as the absolute difference between the estimation of water content using the smooth or roughness model and the GPR-derived water content for the same water content level but with a smooth surface. Following the results presented in Lambot et al. (2004b), the radar approach can indeed be used as a reference to accurately estimate the medium permittivity for the smooth case and this experimental setup. In all cases, the use of the roughness model significantly decreases the estimation errors, with variable benefits depending on actual water content. With the roughness model, the error is

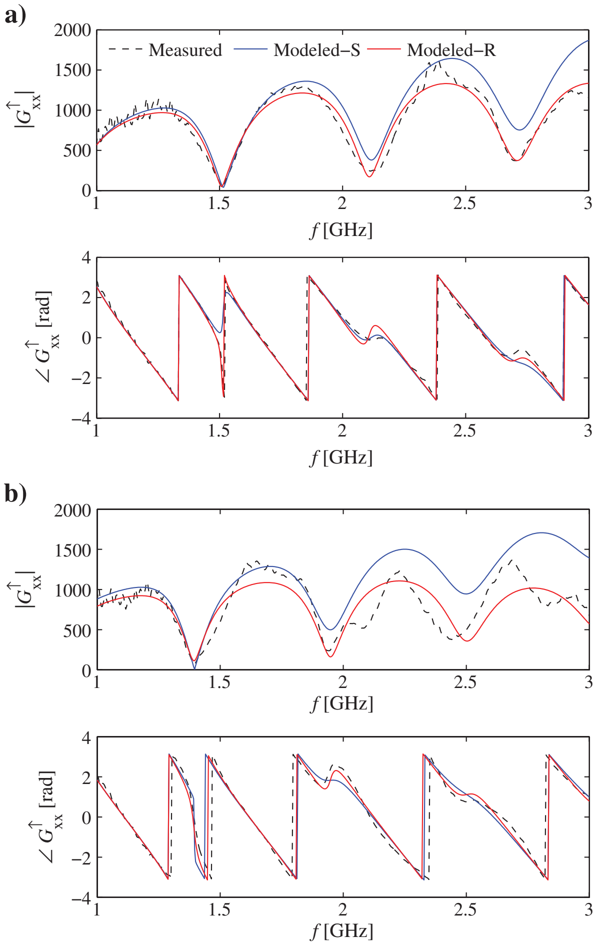

Figure 4. Measured (dashed black line) and modeled (Modeled-S: without using a roughness correction and Modeled-R: with a roughness correction; solid blue and red lines, respectively) amplitude and phase of the frequency-domain Green's function. Data are presented for two water content and roughness height combinations ($\theta = 0.15$ m^3 m^{-3}-$s_r = 0.33$ cm (a), and $\theta = 0.20$ m^3 m^{-3}-$s_r = 0.88$ cm (b)).

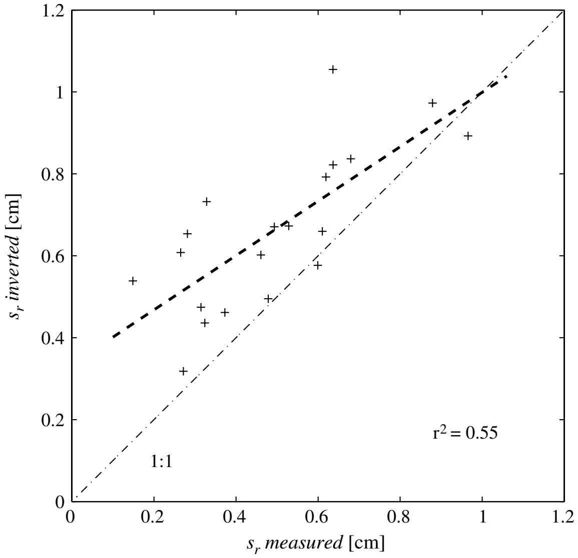

Figure 5. Standard deviation of the GPR-derived roughness amplitude with respect to the real values.

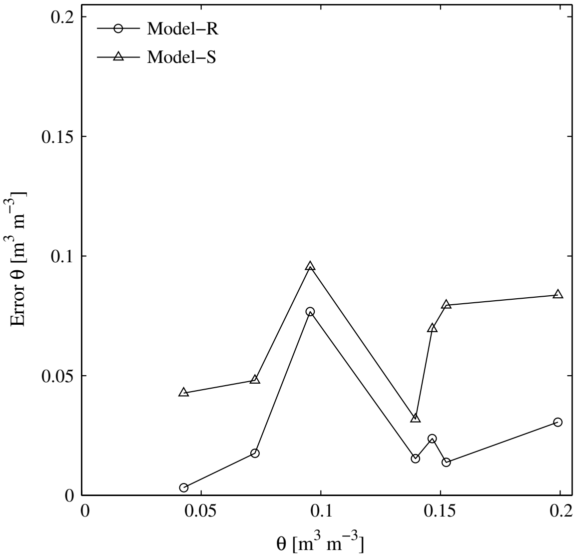

Figure 6. Error in the estimation of water content θ with the surface reflection inversion using the roughness model (Model-R) and the smooth model (Model-S).

1.2–13.2 times smaller compared to the smooth model. The RMS in terms of water content is 0.068 $m^3 m^{-3}$ when considering the smooth model, while with the roughness model the RMS is only 0.034 $m^3 m^{-3}$. In this last case, the roughness was known a priori.

To evaluate the impact of the unknown roughness on the water content retrieval, inversions were also performed using the roughness model and by assuming the roughness unknown (equation 3, $\mathbf{b} = [\varepsilon_r, s_r]$). The RMS in terms of water content is 0.057 $m^3 m^{-3}$, which is similar to the results obtained without accounting for roughness, i.e., with the smooth model. The roughness model significantly improves the retrieval of the water content compared to the smooth model when roughness is known. However, without a priori knowledge of the roughness, the accuracy of the retrieval does not differ significantly between the two models. Similar results were obtained for the lower roughness levels, but with smaller effects.

CONCLUSIONS

The Ament model accounting for scattering losses in the specular direction for rough surfaces was applied to invert off-ground GPR data using Lambot's model. Full-waveform inversion permitted simultaneous reconstruction of the sand dielectric permittivity and the standard deviation of the surface roughness. For this inversion, information about the soil layering was assumed to be known. A practical field inversion strategy based on surface reflection permitted the retrieval of the surface permittivity with a significantly higher accuracy compared to a smooth model. However, in that case, roughness should be independently measured, e.g., by a laser profiler. The proposed method appears to be promising for soil surface moisture mapping in reasonably rough environments (roughness amplitude $< 1/4$ of the wavelength).

ACKNOWLEDGMENTS

This work was supported in part by the Transregional Collaborative Research Centre 32 funded by the DFG (Deutsche Forschungsgemeinschaft) and in part by the FNRS (Fonds National de la Recherche Scientifique, Belgium). The authors are particularly grateful to Khan Zaib Jadoon of the Agrosphere Institute, Forschungszentrum Jülich, for his help during the project. Finally, we also thank the anonymous reviewers for their constructive comments.

REFERENCES

Ament, W. S., 1953, Toward a theory of reflection by a rough surface: Proceedings of the Institute of Radio Engineers, **41**, no. 1, 142–146, doi: 10.1109/JRPROC.1953.274171.

Baghdadi, N., M. Zribi, C. Loumagne, P. Ansart, and T. P. Anguela, 2008, Analysis of TerraSAR-X data and their sensitivity to soil surface parameters over bare agricultural fields: Remote Sensing of Environment, **112**, no. 12, 4370–4379, doi: 10.1016/j.rse.2008.08.004.

Beckmann, P., and A. Spizzichino, 1987, The scattering of electromagnetic waves from rough surfaces: Springer Verlag.

Fung, A. K., Z. Li, and K. S. Chen, 1992, Backscattering from a randomly rough dielectric surface: IEEE Transactions on Geoscience and Remote Sensing, **30**, no. 2, 356–369, doi: 10.1109/36.134085.

Giannopoulos, A., and N. Diamanti, 2008, Numerical modelling of ground-penetrating radar response from rough subsurface interfaces: Near Surface Geophysics, **6**, 357–369.

Huisman, J. A., S. S. Hubbard, J. D. Redman, and A. P. Annan, 2003, Measuring soil water content with ground penetrating radar: A review: Vadose Zone J., **2**, no. 4, 476–491, doi: 10.2113/2.4.476.

Huyer, W., and A. Neumaier, 1999, Global optimization by multilevel coordinate search: Journal of Global Optimization, **14**, no. 4, 331–355, doi: 10.1023/A:1008382309369.

Jonard, F., L. Weihermüller, K. Z. Jadoon, M. Schwank, H. Vereecken, and S. Lambot, 2011, Mapping field-scale soil moisture with L-band radiometer and ground-penetrating radar over bare soil: IEEE Transactions on Geoscience and Remote Sensing, **49**, no. 8, 2863–2875, doi: 10.1109/TGRS.2011.2114890.

Lagarias, J. C., J. A. Reeds, M. H. Wright, and P. E. Wright, 1998, Convergence properties of the Nelder-Mead simplex method in low dimensions: Siam Journal on Optimization, **9**, no. 1, 112–147.

Lambot, S., M. Antoine, M. Vanclooster, and E. C. Slob, 2006a, Effect of soil roughness on the inversion of off-ground monostatic GPR signal for noninvasive quantification of soil properties: Water Resources Research, **42**, no. 3, W03403, doi: 10.1029/2005WR004416.

Lambot, S., E. Slob, and H. Vereecken, 2007, Fast evaluation of zero-offset Green's function for layered media with application to ground-penetrating radar: Geophysical Research Letters, **34**, no. 21, L21405, doi: 10.1029/2007GL031459.

Lambot, S., E. C. Slob, I. van den Bosch, B. Stockbroeckx, B. Scheers, and M. Vanclooster, 2004a, Estimating soil electric properties from monostatic ground-penetrating radar signal inversion in the frequency domain: Water Resources Research, **40**, no. 4, W04205, doi: 10.1029/2003WR002095.

Lambot, S., E. C. Slob, I. van den Bosch, B. Stockbroeckx, and M. Vanclooster, 2004b, Modeling of ground-penetrating radar for accurate characterization of subsurface electric properties: IEEE Transactions on Geoscience and Remote Sensing, **42**, no. 11, 2555–2568, doi: 10.1109/TGRS.2004.834800.

Lambot, S., L. Weihermüller, J. A. Huisman, H. Vereecken, M. Vanclooster, and E. C. Slob, 2006b, Analysis of air-launched ground-penetrating radar techniques to measure the soil surface water content: Water Resources Research, **42**, no. 11, W11403, doi: 10.1029/2006WR005097.

Landron, O., M. J. Feuerstein, and T. S. Rappaport, 1996, A comparison of theoretical and empirical reflection coefficients for typical exterior wall surfaces in a mobile radio environment: IEEE Transactions on Antennas and Propagation, **44**, 341–351, doi: 10.1109/8.486303.

Marquardt, D. W., 1963, An algorithm for least-squares estimation of nonlinear parameters: Journal of the Society for Industrial and Applied Mathematics, **11**, no. 2, 431–441.

Michalski, K. A., and J. R. Mosig, 1997, Multilayered media Green's functions in integral equation formulations: IEEE Transactions on Antennas and Propagation, **45**, no. 3, 508–519, doi: 10.1109/8.558666.

Moran, M. S., C. D. Peters-Lidard, J. M. Watts, and S. McElroy, 2004, Estimating soil moisture at the watershed scale with satellite-based radar and land surface models: Canadian Journal of Remote Sensing, **30**, no. 5, 805–826, doi: 10.5589/m04-043.

Pinel, N., C. Bourlier, and J. Saillard, 2007, Forward radar propagation over oil slicks on sea surfaces using the ament model with shadowing effect: Progress in Electromagnetics Research-Pier, **76**, 95–126.

Quesney, A., S. Le Hegarat-Mascle, O. Taconet, D. Vidal-Madjar, J. P. Wigneron, C. Loumagne, and M. Normand, 2000, Estimation of watershed soil moisture index from ERS/SAR data: Remote Sensing of Environment, **72**, no. 3, 290–303, doi: 10.1016/S0034-4257(99)00102-9.

Sai, B., and L. P. Ligthart, 2004, GPR phase-based techniques for profiling rough surfaces and detecting small, low-contrast landmines under flat ground: IEEE Transactions on Geoscience and Remote Sensing, **42**, no. 2, 318–326, doi: 10.1109/TGRS.2003.817204.

Seneviratne, S. I., T. Corti, E. L. Davin, M. Hirschi, E. B. Jaeger, I. Lehner, B. Orlowsky, and A. J. Teuling, 2010, Investigating soil moisture-climate interactions in a changing climate: A review: Earth-Science Reviews, **99**, no. 3-4, 125–161.

Slob, E., M. Sato, and G. Olhoeft, 2010, Surface and borehole ground-penetrating-radar developments: Geophysics, **75**, no. 5, A103–A120, doi: 10.1190/1.3480619.

Slob, E. C., and J. Fokkema, 2002, Coupling effects of two electric dipoles on an interface: Radio Science, **37**, 1073, doi: 10.1029/2001RS002529.

Ulaby, F. T., M. K. Moore, and A. K. Fung, 1982, Microwave remote sensing: Active and passive, volume ii: Radar remote sensing and surface scattering and emission theory: Artech House.

van der Kruk, J., H. Vereecken, N. Diamanti, and A. Giannopoulos, 2010, Influence of interface roughness and heterogeneities on the waveguide inversion of dispersive GPR data: Presented at the 13th International Conference on Ground Penetrating Radar, IEEE.

Vereecken, H., J. A. Huisman, H. Bogena, J. Vanderborght, J. A. Vrugt, and J. W. Hopmans, 2008, On the value of soil moisture measurements in vadose zone hydrology: A review: Water Resources Research, **44**, W00D06, doi: 10.1029/2008WR006829.

Verhoest, N. E. C., H. Lievens, W. Wagner, J. Alvarez-Mozos, M. S. Moran, and F. Mattia, 2008, On the soil roughness parameterization problem in soil moisture retrieval of bare surfaces from synthetic aperture radar: Sensors, **8**, no. 7, 4213–4248, doi: 10.3390/s8074213.

Yarovoy, A. G., C. N. Vazouras, J. G. Fikioris, and L. P. Ligthart, 2004, Numerical simulations of the scattered field near a statistically rough air-ground interface: IEEE Transactions on Antennas and Propagation, **52**, no. 3, 780–789, doi: 10.1109/TAP.2004.825499.